

“© 2007 IEEE. Personal use of this material is permitted. Permission from IEEE must be obtained for all other uses, in any current or future media, including reprinting/republishing this material for advertising or promotional purposes, creating new collective works, for resale or redistribution to servers or lists, or reuse of any copyrighted component of this work in other works.”

Development of a High Speed Permanent Magnet Motor for Driving Embroidery Machines

J. X. Chen¹, Y. G. Guo², and J. G. Zhu²

¹College of Electromechanical Engineering, Donghua University, Shanghai, 200051, China

²Faculty of Engineering, University of Technology, Sydney, P.O. Box 123, Broadway, NSW 2007, Australia

Introduction

Permanent magnet (PM) motors have found wide applications in industrial and domestic appliance drive market because of their advantages such as high efficiency, high torque-to-volume ratio, and high drive performance. This paper presents the development of a high speed PM brushless DC motor for driving embroidery machines. In the design of the motor, the magnetic field finite element analysis (FEA) was conducted to calculate the key motor parameters such as the air gap flux, back electromotive force (*emf*), and inductance, etc. Based on the numerical magnetic field analysis, a modified incremental energy method (MIEM) is introduced to effectively calculate the self and mutual inductances of the stator windings. The motor prototype has been constructed and tested with both a dynamometer and a high speed embroidery machines, which validates successfully the theoretical calculations.

Motor Configuration and Major Dimensions

Fig.1 illustrates the magnetically relevant parts of the motor. The laminated stator has 12 slots, in which the three phase single-layer windings are placed. The rotor core and shaft are made of solid mild steel, and four pieces of PMs are mounted and bound on the surface of the rotor. The stator core has an inside diameter of 38 mm, outside diameter of 76 mm, and axial length of 38 mm. The main air gap length and the height of the PMs along the radial magnetization direction are chosen as 1 mm and 2.5 mm, respectively. The motor is driven by a brushless DC control scheme, delivering an output torque of 1.6 Nm at the rated speed of 5000 rev/min.

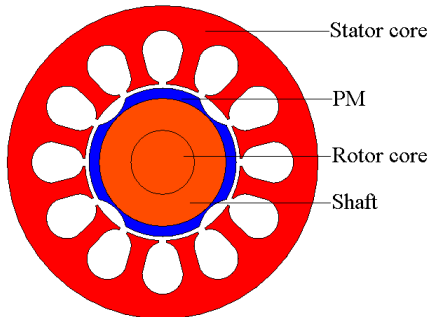


Fig.1 Cross section of high speed PM motor

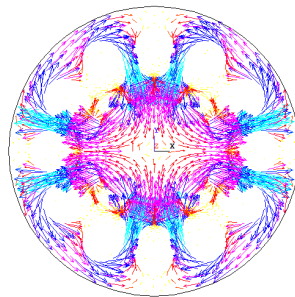


Fig.2 Plot of no-load magnetic flux density vectors

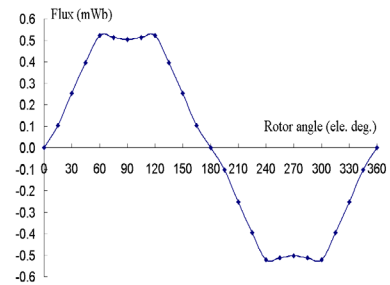


Fig.3 Flux linking a coil versus rotor angle due to rotor PMs

Computation of Motor Parameters and Performance

Fig.2 illustrates the magnetic field distribution at no-load at the rotor position of Fig.1, from which the phase winding flux produced by the rotor PMs, back *emf*, and cogging torque can be determined. The curves of these parameters against the rotor angular position or time can be obtained by a series of magnetic field FEAs at different rotor positions. Fig.3 shows the no-load flux linking a coil (two coils form a phase winding) at different rotor positions. By the discrete Fourier transformation, the magnitude of the fundamental of the coil flux was calculated as $\phi_1=0.543$ mWb, and the *emf* constant can then be determined as 0.2457 Vs/rad, by

$$K_E = \frac{p}{2} N_s \frac{\phi_1}{\sqrt{2}} \quad (1)$$

where $p=4$ is the number of poles and $N_s=320$ is the number of turns of a phase winding. The cogging torque curve was also calculated, but it was found very small with a maximum value of 0.014 Nm.

The winding incremental inductances are calculated by a modified incremental energy method, which includes the following steps: (1) For a given rotor position θ , conduct a non-linear field analysis considering the saturation due to the PMs, and save the incremental permeability in each element; (2) Set the remanence of PMs to be zero, and conduct linear field analyses with the saved permeabilities under perturbed stator current excitations, i.e. assigning the 3 phase winding currents as $(i_a, i_b, i_c) = (\Delta i, \Delta i, 0), (\Delta i, 0, \Delta i), (0, \Delta i, \Delta i), (\Delta i, 0, 0), (0, 0, \Delta i),$ and $(0, \Delta i, 0)$, respectively; (3) Calculate the incremental co-energy for each current excitation; and (4) Calculate the incremental inductances by

$$L_{aa}(\theta) = \frac{2W_c(\Delta i, 0, 0, \theta)}{(\Delta i)^2} \quad (2a)$$

$$L_{ab}(\theta) = L_{ba}(\theta) = \frac{W_c(\Delta i, \Delta i, 0, \theta) - W_c(0, \Delta i, 0, \theta) - W_c(\Delta i, 0, 0, \theta)}{(\Delta i)^2} \quad (2b)$$

$$L_{ca}(\theta) = L_{ac}(\theta) = \frac{W_c(\Delta i, 0, \Delta i, \theta) - W_c(0, 0, \Delta i, \theta) - W_c(\Delta i, 0, 0, \theta)}{(\Delta i)^2} \quad (2c)$$

Fig.4 shows the calculated self and mutual incremental inductances at different rotor positions. To predict the motor performance, an equivalent electrical circuit is derived as shown in Fig.5, where E_l , R_l , and X_l are the back *emf*, stator winding resistance, and synchronous reactance which equals the self reactance plus half of the mutual reactance, and V_l and I_l are the stator phase voltage and current, respectively. The motor is operated in the optimum brushless DC operating mode, i.e. I_l in phase with E_l . Fig.6 illustrates the torque/speed curves with different values of terminal voltage.

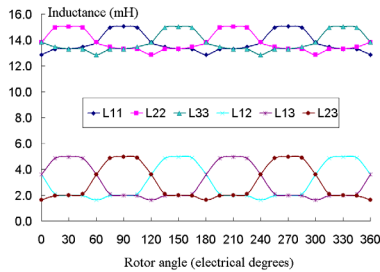


Fig.4 Inductances versus rotor angle

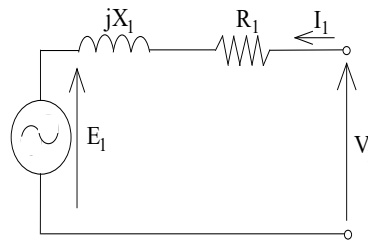


Fig.5 Per-phase equivalent electrical circuit

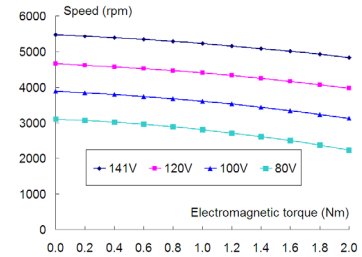


Fig.6 Torque/speed curves

Experimental Validation

A motor prototype has been constructed and tested with a brushless DC control scheme to validate the theoretical calculations. The back *emf* was measured at different rotor speeds and the experimentally determined *emf* constant is 0.2464 Vs/rad, very close to the theoretical value. Other parameters, such as the inductances and torque/speed curves are also in substantially agreement with the theory.

Conclusion

A high speed PM motor has been developed for driving embroidery machines by using magnetic field analysis. A modified incremental energy method is introduced for calculating the self and mutual inductances of the phase windings. The calculations of motor parameters and performance are validated by the experimental results on the prototype. More theoretical and experimental results will be reported in the full paper.